LATVIAN JOURNAL OF PHYSICS
AND TECHNICAL SCIENCES
2026, N 2

DOI: 10.2478/lpts-2026-0009

COMPARATIVE ANALYSIS OF SOLAR RADIATION MEASUREMENTS, MODEL SIMULATIONS, AND REANALYSIS DATA IN URBAN AREAS

J. Sennikovs[1,2], S. Gendelis[2,]*, U. Bethers[1]

[1]Centre for Process Analysis and Research, Ltd,
4 Kīpsalas Str., Riga, LV-1048, LATVIA
[2]University of Latvia,
Faculty of Science and Technology,
Institute of Numerical Modelling
3 Jelgavas St., Riga, LV-1004, LATVIA
*e-mail: stanislavs.gendelis@lu.lv

The study presents a comparative analysis of solar radiation data from ground-based measurements conducted at the Botanical Garden in Riga. The measurements, recorded at one-minute intervals, were compared with corresponding datasets from the Copernicus Atmosphere Monitoring Service (CAMS) Radiation Service, the DWD-ICON numerical weather prediction model, and the ERA5 reanalysis. The high temporal resolution of the ground-based data enables the detection of short-term fluctuations caused by transient cloud events, which are often smoothed out in model or reanalysis datasets with coarser (15-minute to hourly) resolution. Results show that CAMS generally reproduces the seasonal and diurnal patterns of global horizontal irradiance (GHI) with good accuracy but tends to overestimate peak radiation values, while ERA5 underestimates GHI under clear-sky summer conditions. To improve comparability, a LIDAR-based shading correction was applied using local obstruction data (vegetation and buildings), which increased the overall accuracy index up to 84 %. The findings highlight the importance of integrating high-resolution ground-based measurements with reanalysis and model outputs for solar energy applications in urban environments, where local shading and fine-scale atmospheric dynamics play a critical role.

Keywords*: CAMS, DWD-ICON, ERA5, ground-based validation LIDAR, reanalysis, shading correction, solar radiation.*

1. INTRODUCTION

Accurate estimation of solar radiation is fundamental for solar-energy assessment, building performance modelling, and studies of surface–atmosphere processes in mid-latitudes. In urban settings, fine-scale effects from vegetation, buildings, and local air quality introduce spatial and temporal variability that large-scale datasets may not resolve well.

Among widely used sources, the Copernicus Atmosphere Monitoring Service (CAMS) Radiation Service provides near-real-time and historical surface irradiance by combining satellite cloud retrievals with modelled aerosols and trace gases [1]. The DWD-ICON numerical weather prediction model supplies forecast time series of global, direct, and diffuse irradiance at hourly resolution [2]. The ERA5 reanalysis offers globally consistent hourly radiation fields on a 0.25° grid, suitable for climatological and operational applications alike [3]. For Latvia specifically, national assessments have reported measured irradiance levels that support feasible solar deployment, underscoring the need for robust validation frameworks [4].

Despite broad uptake, model and reanalysis products may misrepresent local conditions where shading, urban geometry, and sub-grid cloud dynamics dominate. High-frequency ground observations therefore remain essential for evaluating these datasets, especially in complex urban fabrics. In the present study, global horizontal irradiance (GHI) from CAMS [1], DWD-ICON [2], and ERA5 [3] is compared with one-minute ground measurements collected at the Botanical Garden in Riga, Latvia (hereafter the measurement site) – see Fig. 1. The influence of local obstructions is quantified using a LIDAR-based shading model derived from GeoRiga data [5], with additional reference information from the Latvian Environment, Geology and Meteorology Centre (LVĢMC) [6].

The study makes three contributions: (i) benchmarking CAMS, DWD-ICON, and ERA5 against high-resolution observations in a northern European city; (ii) diagnosing systematic biases – such as CAMS peak overestimation and ERA5 clear-sky underestimation – in the context of temporal resolution and parameterisation; and (iii) demonstrating that a site-specific, LIDAR-based shading correction materially improves agreement, yielding accuracy indices up to ~84 %. These findings complement prior European validations of CAMS and ERA5 [7], [8] and align with urban solar studies that incorporate digital surface models and LIDAR for shading-aware assessments [9]–[12].



Fig. 1. Location of a measurement site in Riga, Latvia (© GeoRiga).

2. EXPERIMENTAL

2.1. Data Sources

This study used four primary sources of solar-radiation data: (1) one-minute ground measurements; (2) the CAMS Radiation Service [1], [6]; (3) the DWD-ICON numerical weather prediction model [2]; and (4) the ERA5 reanalysis [3]. Additional meteorological reference information was obtained from the LVĢMC [6]. Global horizontal irradiance (GHI) was recorded at the Botanical Garden in Riga (hereafter the measurement site) using a calibrated pyranometer mounted in the horizontal plane. The dataset covers 2020–2025 with a native one-minute resolution, which captures transient variability associated with moving clouds and short-lived shading events.

The CAMS Radiation Service provides surface irradiance by combining satellite cloud retrievals with modelled aerosols and trace gases (Heliosat-4/McClear), delivering clear-sky and all-sky time series at point locations with nominal 1-minute time step and on a 0.1° grid [1]. For the present analysis, point time series at the measurement-site coordinates were retrieved at 1-minute resolution and then temporally aligned (and, where required, aggregated to 1-hour) to ensure like-for-like comparison with the ground data. DWD-ICON provides forecast time series of GHI, direct normal irradiance (DNI), and diffuse horizontal irradiance (DHI) at hourly resolution [2]. Historical forecasts were obtained via the Open-Meteo interface, retaining non-overlapping forecasts by keeping the most recent issue for each timestamp to avoid duplication. ERA5 offers hourly radiation fields on a 0.25° grid [3]. Available components include GHI and DHI. DNI was derived from ERA5 fields using the solar-elevation angle; DHI was also inferred where required to ensure consistent component availability across datasets. Time series were bilinearly interpolated to the measurement-site coordinates.

2.2. Shading Analysis and Correction

High-resolution LIDAR point-cloud data from GeoRiga were used to quantify local obstructions [6]. The survey (August–September 2022) combined aerial and terrestrial laser scanning, with 200–300 points m^{-2} in open areas. Points classified as high vegetation (class 5), buildings (class 6), and wire-structure insulators (class 16) were selected. Mean and maximum surface rasters were generated at 0.2 m spacing and used in a line-of-sight (LOS) analysis over the full annual solar path.

Hourly shading coefficients were computed to represent the fraction of the sky dome unblocked by surrounding features. Full shading was assumed when the Sun lay below the mean surface height; between the mean and maximum heights, a partial transmittance of 0.9 was applied to represent porous canopies and edge effects. The resulting coefficients were applied multiplicatively to model/reanalysis GHI to produce shading-corrected series, subsequently compared with observations at the measurement site.

2.3. Statistical Evaluation

Performance was assessed using commonly adopted solar-radiation metrics [7]: mean absolute error (MAE), root mean square error (RMSE), mean absolute per-

centage error (MAPE), coefficient of determination (R^2), and an overall forecast accuracy index (AI). Metrics were computed for raw and shading-corrected datasets to quantify the impact of obstruction modelling.

2.4. Temporal Aggregation

As dataset resolutions differ – 1 minute for the ground measurements, 1 minute for CAMS, and 1 hour for DWD-ICON and ERA5 – all series were harmonised to hourly resolution for direct comparison. Ground-based and CAMS data were aggregated to hourly means, whereas DWD-ICON and ERA5 hourly values were used as provided (no interpolation). Note that CAMS also permits direct download of pre-aggregated hourly series; reconstructing hourly values from the 1-minute data yields equivalent results and was adopted here for consistency with the ground data workflow.

3. RESULTS

3.1. GHI: Ground-Based Measurements and CAMS

Ground-based measurements at the measurement site were compared with corresponding estimates from CAMS, DWD-ICON, and ERA5 over 2023–2024. All datasets reproduced the broad diurnal and seasonal variability of global horizontal irradiance (GHI), but systematic differences in magnitude and temporal response were evident. Long-term time series further show that CAMS captures the seasonal evolution of GHI but smoothes short-term variability, with small clear-sky biases also apparent (Fig. 2).

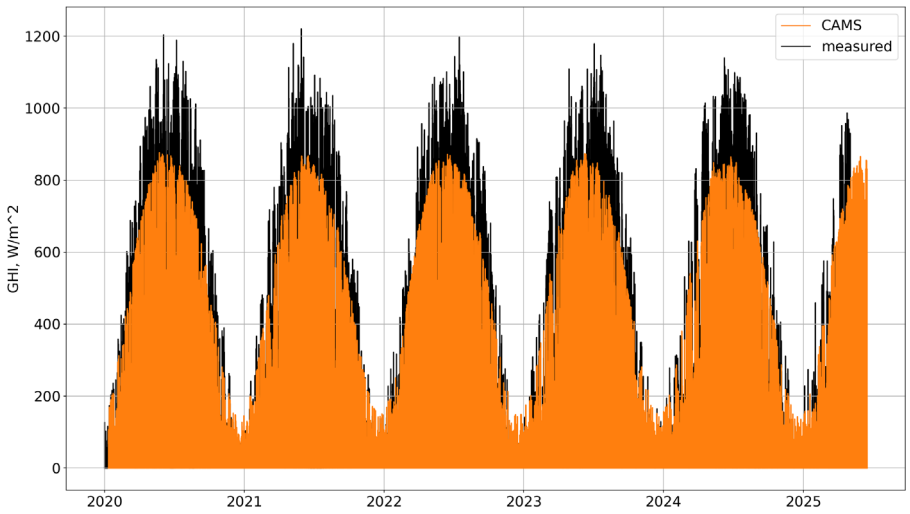


Fig. 2. CAMS and measured GHI: CAMS captures the seasonal cycle but smoothes short-term peaks.

Although CAMS provides nominal one-minute series, the underlying satellite inputs operate at approximately 15-minute resolution, leading to temporal smoothing relative to the one-minute observations [1]. As a result, short-lived peaks associated with cloud-edge effects are reduced in CAMS. This behaviour is illustrated for a partly cloudy summer day in Fig. 3, where rapid irradiance fluctuations in the measurements are muted in CAMS, while daily totals remain comparable. CAMS smoothes rapid fluctuations from passing clouds. Differences are evident also on clear-sky days, potentially due to atmospheric-transparency assumptions or local air pollution.

Example of a summer day – 6 June 2024, with variable cloud cover, a relatively typical scene in such cases is shown in Fig. 4. The image shows measurement and model data, as well as the corresponding satellite image with clearly visible clouds. Another example with some clouds in the afternoon is shown in Fig. 5. A day with high clouds is shown in Fig. 6 – CAMS data reflects their effect, but insufficiently.

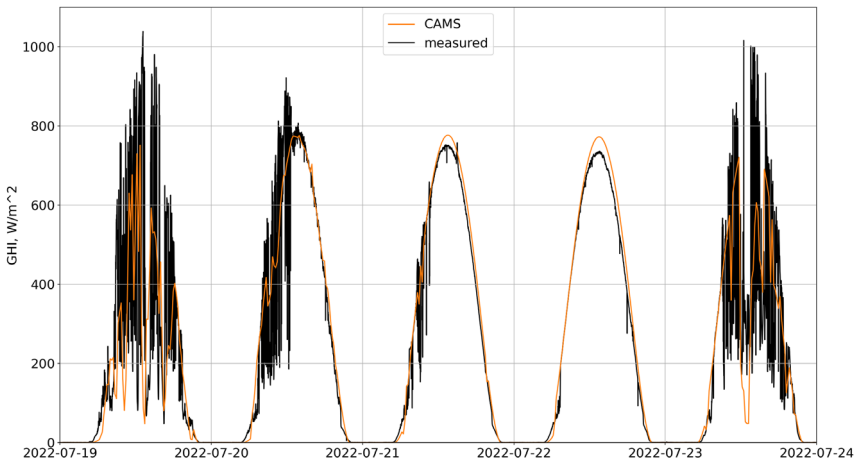


Fig. 3. CAMS and measured GHI for partly cloudy (June 20) and clear-sky (June 22) days.

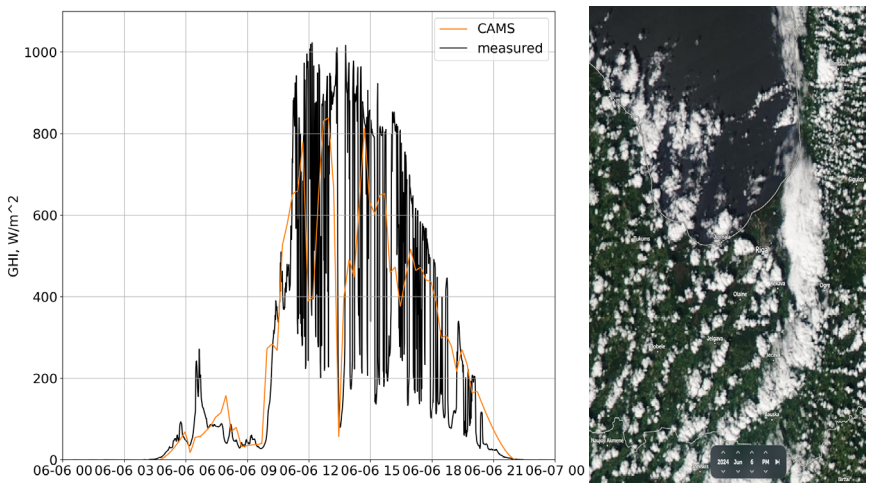


Fig. 4. Measured GHI and CAMS on a cloudy day (© Zoom Earth, EUMETSAT, MeteoSat).

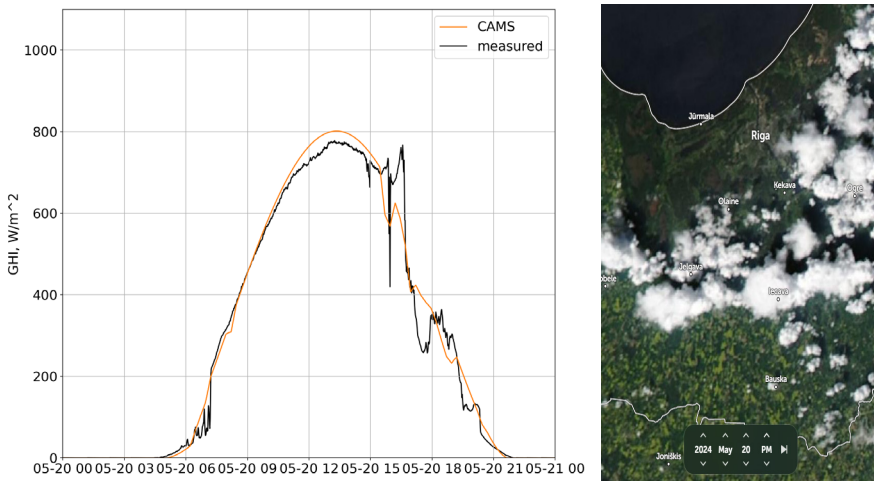


Fig. 5. Measured GHI and CAMS on a day with a few afternoon clouds (© Zoom Earth, EUMETSAT, MeteoSat).

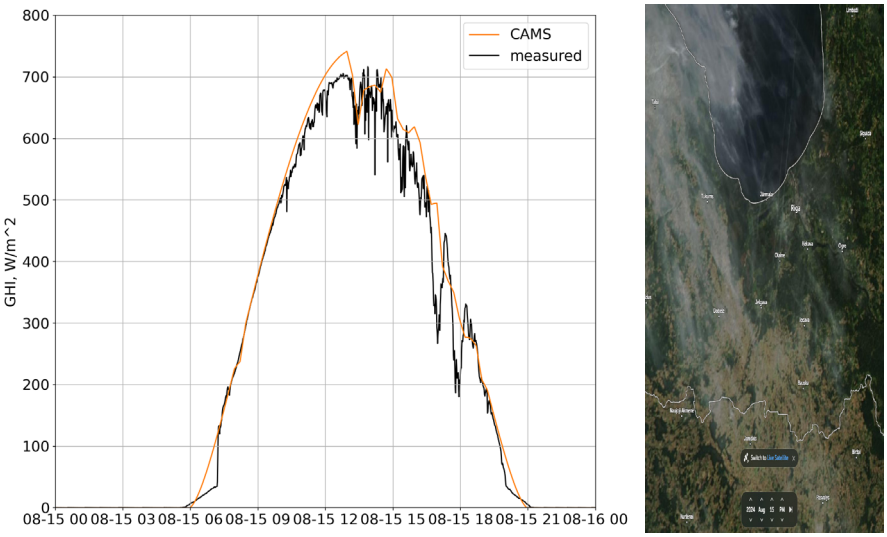


Fig. 6. Measured GHI and CAMS on a day with high clouds (© Zoom Earth, EUMETSAT, MeteoSat).

3.2. GHI: Comparison of measurements, CAMS, DWD-ICON and ERA5 Datasets – Hourly Data

Ground-based global horizontal irradiance (GHI) at the measurement site was evaluated against CAMS, DWD-ICON, and ERA5 under representative clear, cloudy, and shading conditions. GHI analysis for two consecutive clear summer days (Fig. 7) shows that all datasets reproduced the diurnal cycle. CAMS overestimated around solar noon and towards sunset, whereas DWD-ICON and ERA5 aligned more closely with the measured peak but diverged during the morning hours, consistent with

low solar elevation and sensitivity to aerosol/cloud assumptions at dawn. This behaviour matches known CAMS limitations in capturing short-lived irradiance peaks due to its temporal processing method, whereas ERA5 deviations stem from its coarse spatial resolution [3], [7], [8].

On a day with variable cloud cover (Fig. 8), CAMS partially captured cloud passages but smoothed minute-scale variability typical of one-minute measurements. DWD-ICON and ERA5 diverged more strongly on the sub-daily scale, as hourly outputs could not resolve transient cloud fields; timing mismatches produced alternating under- and overestimation, while daily totals remained broadly comparable.

A clear-sky winter day at the beginning of January, clearly affected by shading (Fig. 9), demonstrates that local obstructions (buildings and vegetation) produced pronounced morning and late-afternoon shade on the instrument that none of the datasets captured explicitly. Consequently, all three sources reported higher irradiance than measured. The pattern is consistent with the LIDAR-derived obstruction context described in the next chapter. One month later, in February (Fig. 10), shading was smaller in the morning hours but still present during afternoon. The model/reanalysis curves retained an idealised clear-sky diurnal profile, whereas the measurements showed partial shading and perturbations from the tree canopy.

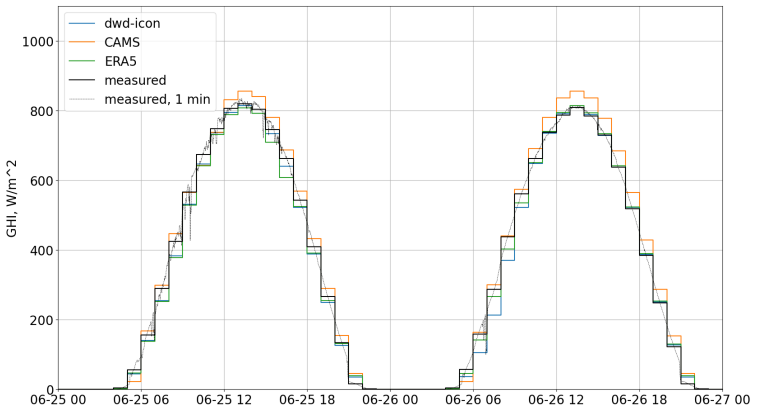


Fig. 7. GHI comparison for two clear summer days.

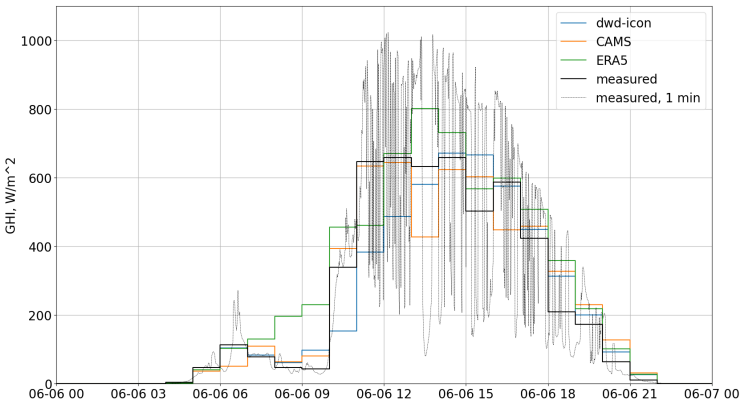


Fig. 8. GHI comparison for a day with variable cloudiness.

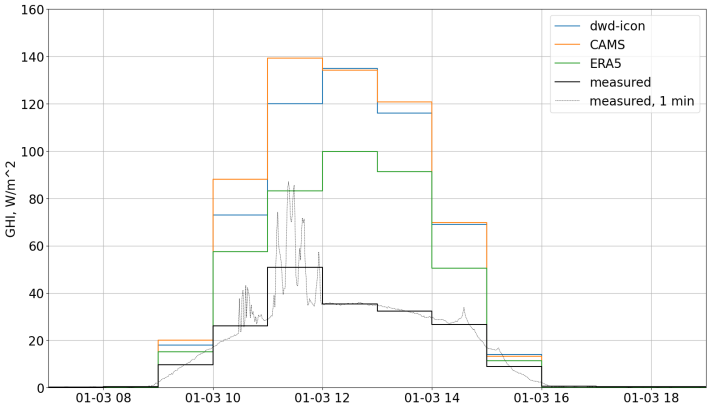


Fig. 9. GHI comparison for a clear winter day (with local obstructions).

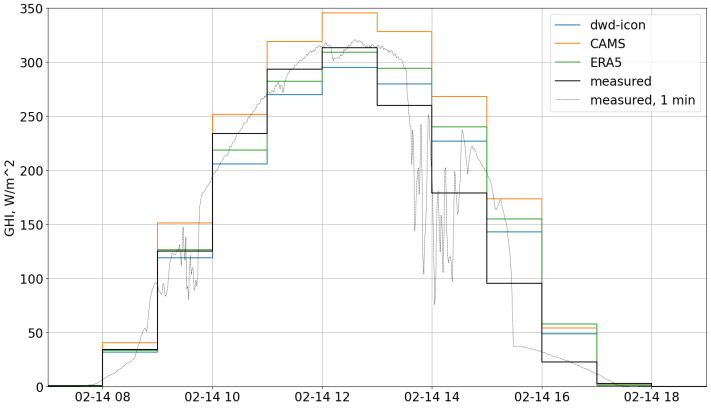


Fig. 10. GHI comparison for a clear winter day (local obstructions in the afternoon).

3.3. GHI: Comparison of measurements, CAMS, DWD-ICON and ERA5 Datasets – Monthly Data

The averaged monthly mean GHI for 2020–2025 (Fig. 11) shows that all datasets reproduce the annual cycle with small inter-annual variability. Systematic winter differences are evident: measured GHI is consistently lower in November–February than any of the three datasets, reflecting site-specific shading at low solar elevation. For the rest of the yearly cycle, the series remain close – CAMS generally tracks the measurements, DWD-ICON is slightly higher during peak-sun months, and ERA5 shows the largest departures around late spring and early summer. Consistent with the accuracy-index analysis, months dominated by cloudy days yield poorer agreement than clear-sky months, with lower GHI accuracy indices during cloudier periods (see next chapter).

Using the modelled-to-measured monthly mean ratio highlights the same tendencies (Fig. 12). In the darker months, ratios fall below unity because the measured values are reduced by site-specific shading at low solar elevation. DWD-ICON maintains good monthly means and

stays close to unity across most months. By contrast, ERA5 departs in spring and summer, consistent with under-represented cloudiness at the site scale (a grid/representativeness effect), which elevates its monthly GHI relative to the measurements. Overall monthly GHI from CAMS, DWD-ICON, and ERA5 shows relatively good agreement with the ground measurements, while clarifying when departures are most likely – winter due to shading and short daylight period, and late spring–summer where ERA5's grid/parameterisation effects become apparent.

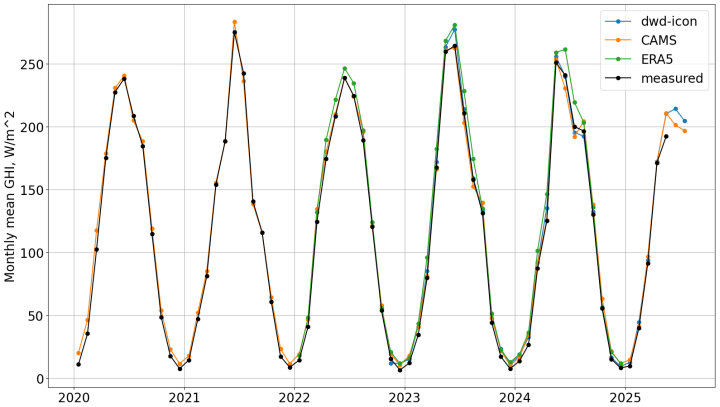


Fig. 11. Monthly GHI measured data and CAMS/DWD-ICON/ERA5 models.

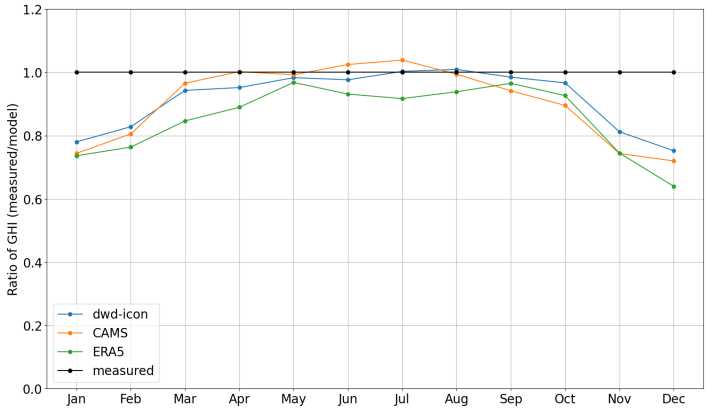


Fig. 12. Averaged ratio of GHI for measurements and CAMS/DWD-ICON/ERA5 models.

3.4. Accuracy Index for CAMS, DWD-ICON and ERA5 Datasets

The daily GHI accuracy index for 2023–2024 (Fig. 13) shows a clear seasonal distribution. Values cluster around ~70–95 % from late spring to early autumn, with day-to-day variability driven by transient cloud fields with clear sky days generally having higher accuracy index. In mid-winter (November–February), frequent low – occasionally even negative – daily values occur across all datasets, reflecting the combined effects of low solar elevation, frequent cloud, and site-specific shading that

lead to lower measured signal relative to model/reanalysis outputs. Spread between datasets increases during unsettled periods; CAMS tends to occupy the upper part of the distribution on clear or partly cloudy days, whereas ERA5 more often falls to the lower end in winter and early spring.

The monthly accuracy index averaged from 2023 and 2024 data (Fig. 14) condenses these patterns: indices rise from winter minima to peaks in May–June (~85–90 %), then decline gradually through autumn. CAMS attains the highest monthly values across most of the bright season, DWD-ICON follows closely with small month-to-month departures, and ERA5 remains systematically lower – especially in January–March and again in late autumn – consistent with the behaviour discussed earlier for coarse-grid and cloud-parameterisation effects. The lowest indices in November–December coincide with maximum shading impact at the measurement site and the greatest cloud variability. Taken together, the daily and monthly indices confirm that agreement among datasets is strongest under clear-sky, high-Sun conditions, and weakest during winter when shading and cloud variability dominate. The indices with applied corrections, shown in this figure as dotted lines, will be described later.

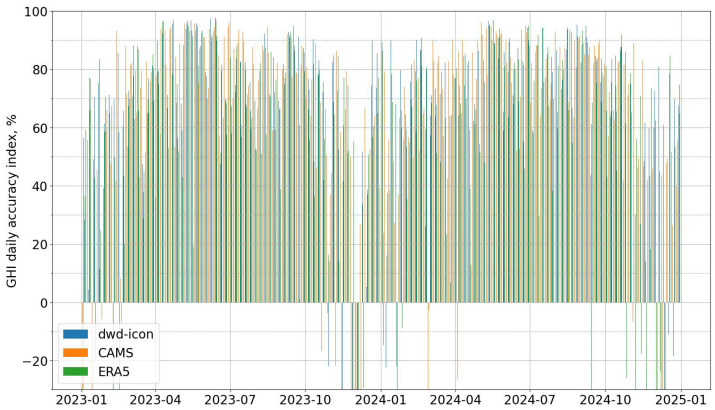


Fig. 13. Daily GHI accuracy index.

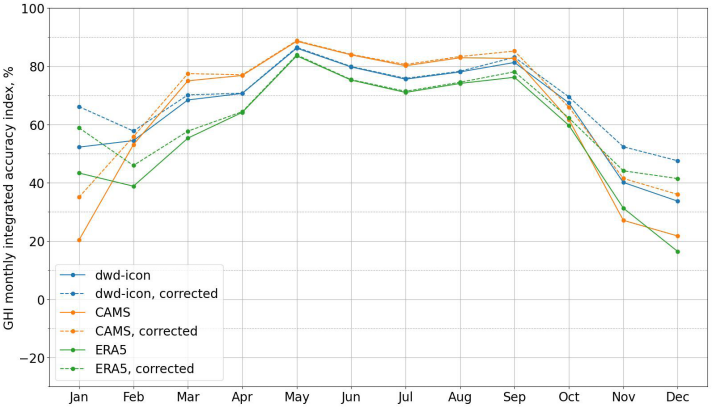


Fig. 14. Monthly GHI accuracy index with/without shading correction.

3.4. GHI: Influence of Local Shading on Model Accuracy

Site-specific effects also contributed to differences. Partial shading from nearby vegetation and buildings, along with reflections from surrounding surfaces, influenced measured GHI. Even under clear-sky conditions, discrepancies persisted between modelled and measured values.

Local obstructions were quantified using a LIDAR-based method. The spatial map of major obstacles is shown in Fig. 15, derived from LIDAR elevation data around the measurement site (see also Fig. 1), while the resulting annual shading diagram is presented in Fig. 16, with permanent sectors (dark grey) largely associated with buildings and partial or seasonal sectors (light grey) mainly due to vegetation. From diagram it is clearly evident, that sensor is in shade during large parts of the day for two months around winter solstice. Shading also is pronounced in the afternoon for nearly half a year and in early morning and late evening during the whole year.

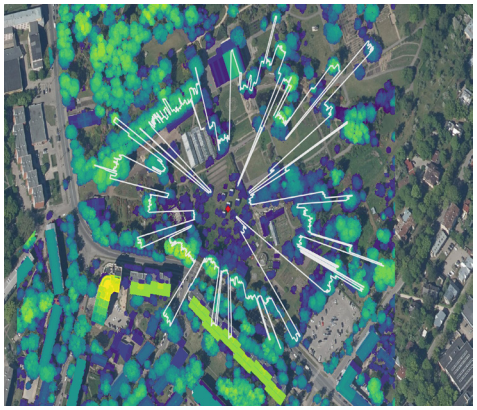


Fig. 15. Spatial distribution of LIDAR-derived elevation data and shadings around the measurement site.

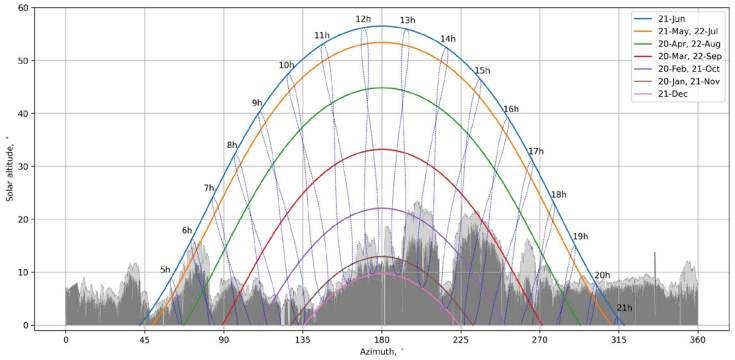


Fig. 16. Annual shading diagram with shading mask for the measurement site. Dark grey areas indicate permanent obstructions; light grey areas represent partial or variable shading.

Figure 17 illustrates several systematic effects. First, the onset of measured irradiance in the morning is delayed relative to CAMS, consistent with tree shading at low solar elevation. Secondly, intermittent mid-day depressions in the measured curve

indicate partial, moving-canopy shading that CAMS cannot represent. Finally, the measured signal decays markedly earlier in the late afternoon because the Sun becomes obstructed by nearby buildings, whereas CAMS maintains an unobstructed, quasi-symmetric clear-sky profile. These features align with the annual shading sectors derived from the LIDAR analysis and explain part of the winter bias seen in the monthly statistics.

Figure 18 demonstrates the same geometry-driven behaviour across three consecutive clear-sky days in December. The measured GHI exhibits a repeatable morning window with reduced amplitude, followed by a sharp decline around local noon as shadows from the adjacent building fall on the sensor. Afternoon irradiance remains strongly suppressed or absent, while CAMS continues to report an idealised bell-shaped curve. The day-to-day persistence confirms that the losses are primarily geometric rather than meteorological, providing a clear rationale for the improvement observed when applying the LIDAR-based shading coefficients to the model/reanalysis datasets. Operationally, such wintertime obstruction leads to substantial overestimation of daily totals by CAMS (and, by extension, any model that assumes an unobstructed horizon), and it explains the lower accuracy indices during months with low solar elevation.

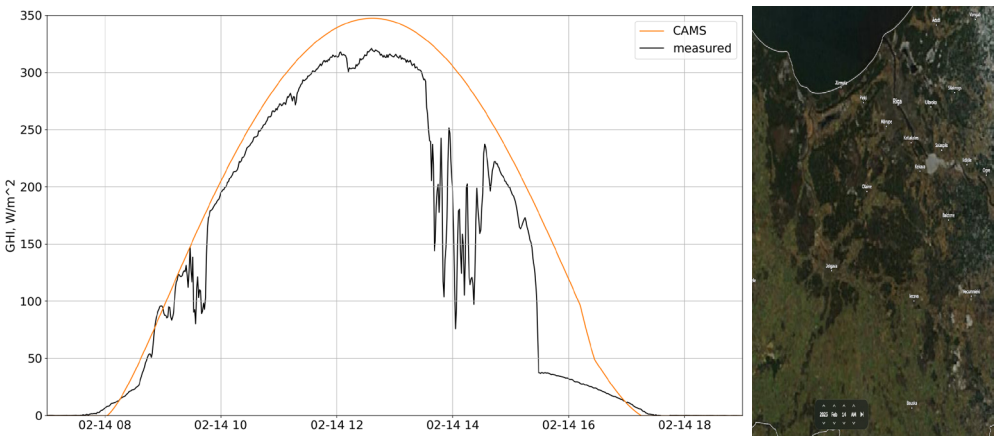


Fig. 17. Measured GHI and CAMS in a clear-sky with shading effects from trees (in the morning and afternoon) and building (last 2 hours) (© Zoom Earth, EUMETSAT, MeteoSat).

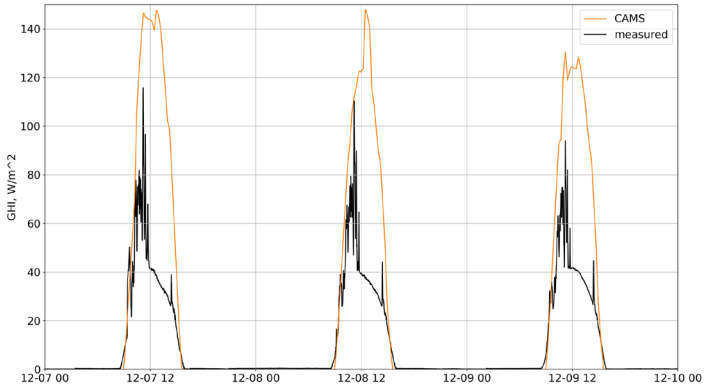


Fig. 18. Shading effect from the adjacent building in the afternoons (7–9 December).

3.5. Calculated Performance Metrics

Quantitative evaluation of measured and modelled GHI values relies on complementary metrics, including mean absolute error (MAE, W/m²), root mean square error (RMSE, W/m²), mean bias (W/m²), the coefficient of determination (R^2), and an integrated overall accuracy index (AI, %) that summarises agreement over time. In this study, AI is defined from the weighted mean absolute percentage error (WMAPE) as 100 − WMAPE (%), where the sums run over all valid hourly time steps in 2023–2024 (nighttime or invalid values excluded) [16], [17]. The standard mean absolute percentage error (MAPE) is easy to interpret but can be severely inflated when actual values are small and is overly sensitive to a few extreme percentage errors. Consequently, for forecasting and evaluation MAPE should be used with great caution, and WMAPE should be preferred wherever possible. R^2 is reported to indicate the fraction of variance in the observations explained by the model fit [18]. Using these indicators on hourly series for 2023–2024 enables a consistent comparison across datasets with different native resolutions and helps isolate the impact of site-specific shading. Calculated metrics for all three datasets (CAMS, DWD-ICON, and ERA5) are summarised in Table 1.

Across the period, all three datasets agree reasonably well with the ground measurements at the measurement site, but with clear differences in skill. Without accounting for local shadings, CAMS attains the highest overall accuracy index (83.3 %), the lowest total percentage deviation (1.9 %), and a small mean bias (+2 W/m²). DWD-ICON performs consistently (accuracy index 80.4 %, mean bias +3 W/m²). ERA5 shows the largest departures (accuracy index 77 %, mean bias +10 W/m²), with a higher average modelled value (125 W/m²) than the measured mean (114 W/m²).

Applying hourly, LIDAR-derived shading coefficients improves agreement for all datasets. The largest gain is for CAMS: the accuracy index increases from 83.3 % to 84.5 %, and mean bias is effectively removed (from +2.2 to approximately 0 W m^{-2}). The overall accuracy index for DWD-ICON rises from 80.4 % to 81.3 %, and for ERA5 from 77.0 % to 78.1 %; ERA5 nevertheless remains the least accurate at this site, consistent with its coarser spatial resolution and parameterisation.

Table 1. Measured and Modelled GHI and Performance Metrics

Measured value, W/m²	114					
Models	Without shadings			With shading corrections		
	DWD-ICON	*CAMS*	*ERA5*	*DWD-ICON*	*CAMS*	*ERA5*
Modelled value, W/m²	117.7	116.5	124.6	115.6	114.3	122.0
Mean absolute error (MAE), W/m²	22.4	19.1	26.3	21.4	17.7	25.0
Root mean square error (RMSE), W/m²	50.9	40.2	59.5	50.2	38.7	58.7
Mean bias, W/m²	3.4	2.2	10.3	1.3	-0.1	7.7
Overall accuracy index (AI), %	**80.4 %**	**83.3 %**	**77.0 %**	**81.3 %**	**84.5 %**	**78.1 %**
MAPE, %	72.2 %	72.8 %	75.4 %	68.4 %	68.9 %	71.8 %
R^2	0.931	0.957	0.906	0.933	0.960	0.908

Visualisation of the monthly behaviour of the accuracy index, with and without shading correction is shown in Fig. 14. Values typically exceed ~80 % from late spring to summer, when shading effects are minimal and sky conditions are more stable. During late autumn and winter, the index drops below ~70 %, reflecting the combined influence of low solar elevation, frequent cloud cover, and longer shadows that amplify differences between model/reanalysis datasets and ground observations. Applying the shading correction systematically increases the monthly accuracy index for all datasets, with the most pronounced improvements during months with short daylight and dense tree foliage, when shading effects dominate.

In summary, once site-specific shading is taken into account, CAMS achieves the highest overall performance, DWD-ICON delivers stable and consistent estimates, while ERA5 exhibits seasonally dependent biases. The results demonstrate that incorporating shading-aware preprocessing together with high-frequency ground measurements substantially improves the reliability of urban solar-resource characterisation.

4. DISCUSSION

The analysis of measurements versus CAMS, DWD-ICON and ERA5 reveals how well satellite-derived and modelled datasets can reproduce real-world irradiance dynamics under complex urban conditions. While all datasets successfully capture the seasonal cycle and general irradiance trends, systematic differences emerge that are relevant for shading-affected locations, PV-performance evaluations and urban energy planning. The following discussion interprets these differences, links them to atmospheric or spatial drivers, and assesses their implications for practical solar-resource assessment.

4.1. Model Performance and Bias Interpretation

Among the evaluated datasets, CAMS exhibited the highest overall accuracy and most accurately represented diurnal and seasonal variability. A tendency to slightly overestimate short-term peaks was evident, plausibly linked to interpolation from native ~15-minute satellite inputs and uncertainties in cloud optical thickness parameterisation [1], [7]. This behaviour is compatible with findings reported for Central and Northern Europe, where several studies note peak overestimation under clear-sky/high-transparency conditions [7], [8].

In contrast, ERA5 systematically underestimated irradiance during clear-sky periods. The bias can be partly attributed to its coarse 0.25° grid and grid-cell averaging effects, with the impact most pronounced in summer when high solar elevation increases sensitivity to aerosol assumptions and local transparency [3].

DWD-ICON exhibited intermediate behaviour, combining moderate bias with strong temporal correspondence to observations. Its finer spatial resolution and physically based cloud microphysics enable closer tracking of sub-hourly irradiance patterns, although sensitivity to small-scale cloud dynamics and albedo variability remains evident [19].

4.2. Role of High Temporal Resolution

The 1-minute ground measurements captured rapid irradiance excursions caused by cloud edges, thin-cloud passages, and transient shading that were smoothed in hourly and satellite-derived datasets. This behaviour aligns with previous findings that short-term variability and peaks diminish as averaging windows increase. High temporal resolution is therefore essential for applications in PV ramp-rate analysis, inverter sizing, and grid integration studies where transient variability drives performance constraints [16], [17].

4.3. Influence of Local Shading

The LIDAR-based analysis confirmed permanent and seasonal shading from nearby vegetation and buildings. Incorporating the derived hourly shading coefficients into each dataset's time series improved all performance metrics. The largest improvement was achieved for CAMS, with the overall accuracy index increasing from 83.3 % to 84.5 %, while both DWD-ICON and ERA5 showed smaller but consistent improvements. These findings indicate that refinement of global datasets using site-specific obstruction modelling leads to a more realistic representation of urban irradiance, aligning with similar work using digital surface models in urban PV assessments [9]–[12]. Furthermore, the results show that even coarse-grid datasets can be materially improved when coupled with shading-aware preprocessing. Such hybrid approaches are increasingly used to enhance predictive skill and reduce uncertainty in rooftop PV potential estimation [10]–[12].

4.4. Implications and Limitations

From a practical standpoint, combining high-frequency ground observations with model and reanalysis products improves the reliability of urban solar-resource assessments. Incorporating shading information enables more realistic estimates of PV yield, particularly in dense built environments where obstruction geometry strongly modulates irradiance [9], [12]. The measured irradiance levels are consistent with regional studies indicating that Riga and Latvia have competitive GHI values sufficient to support broader deployment of solar technologies [4].

Several limitations should be acknowledged. The analysis is limited to a single site and a two-year period, and residual discrepancies may arise from unobserved atmospheric parameters such as aerosol composition, humidity or surface reflectivity. Additional measurement sites would help represent the spatial heterogeneity of shading and atmospheric conditions across different urban morphologies.

5. CONCLUSIONS

The comparison of solar-radiation datasets (CAMS, DWD-ICON, and ERA5) with ground-based measurements at the site shows that global horizontal irradiance (GHI) from satellite- and model-based products agrees relatively well with observations. Integrating high-resolution ground measurements with numerical model outputs enables assessment of both large-scale atmospheric effects and local urban influ-

ences such as surface obstructions. The main findings are as follows:

- *Short-term variability*: One-minute ground observations resolve transient irradiance peaks and dips caused by cloud-edge effects and moving shadows, whereas 15-minute to hourly datasets smooth this variability. High temporal resolution is therefore valuable for ramp-rate analysis, PV-performance assessment and grid-integration studies.
- *Dataset behaviour*: CAMS reproduces diurnal and seasonal patterns most accurately overall but tends to overestimate short-lived peaks. DWD-ICON shows intermediate performance with strong temporal correlation to observations, while ERA5 exhibits a systematic clear-sky negative bias, particularly in summer, linked to coarse spatial resolution and radiative-transfer parameterisation.
- *Shading matters*: Applying a LIDAR-based, site-specific shading correction improves all performance metrics. The overall accuracy index increases up to ~84 %, demonstrating that local obstructions (buildings, vegetation) are a dominant contributor to discrepancies between modelled and measured irradiance in urban environments, especially during low-sun periods
- *Urban assessment framework*: Combining ground measurements with model and reanalysis datasets – augmented by shading-aware preprocessing – provides a robust approach for urban solar-resource characterisation, reducing uncertainty in PV siting, yield estimation and forecasting.

In summary, CAMS delivers the best overall performance, DWD-ICON offers robust and stable estimates, and ERA5 shows seasonally dependent biases. Satellite/model/reanalysis products can be reliably applied for solar-energy planning in northern European cities, provided that sub-hour variability and local effects are explicitly addressed. In practice, this means accounting not only for cloud dynamics, but also for site-specific shading from buildings and vegetation, which large-scale models neither represent nor can feasibly represent. Such local obstructions must be characterised and corrected individually – for example, via LIDAR-based shading modelling – to achieve the highest forecasting accuracy. If models are used for PV sizing or energy forecasting without considering local shading, daily totals may be substantially overestimated during winter.

ACKNOWLEDGEMENTS

The study has been supported by the Recovery and Resilience Mechanism the Research No. J.1.7 “Development of a Prototype of an Automated Renewable Energy Generation Forecasting Engineering System” ID. No. 5.1.1.2.i.0/2/24/A/CFLA/008, the Mechanical Engineering Competence Centre support to research.

REFERENCES

1. Copernicus Atmosphere Monitoring Service. (2021). *User guide to the CAMS radiation service (CRS)*. (PDF) https://atmosphere.copernicus.eu/sites/default/files/2022-01/CAMS2_73_2021SC1_D3.2.1_2021_UserGuide_v1.pdf?utm_source=chatgpt.com

2. Deutscher Wetterdienst. (2024). *ICON numerical weather prediction model: Forecast data and documentation*. https://www.dwd.de/EN/ourservices/nwp_forecast_data/nwp_forecast_data.html
3. Hersbach, H., Bell, B., Berrisford, P., Hirahara, S., Horanyi, A., Muñoz-Sabater, J., … & Thépaut, J.-N.(2020). The ERA5 global reanalysis. *Quarterly Journal of the Royal Meteorological Society, 146*(730), 1999–2049. https://doi.org/10.1002/qj.3803
4. Sakipova, S. E., Jakovics, A., & Gendelis, S. (2016). The potential of renewable energy sources in Latvia. *Latvian Journal of Physics and Technical Sciences, 53*(3), 3–14. https://doi.org/10.1515/lpts-2016-0001
5. GeoRiga. (2022). *LiDAR point cloud (open data)*. https://georiga.eu/atvertie-dati/lidar-punktu-makonis/
6. Latvian Environment, Geology and Meteorology Centre (LVĢMC). (2025). *About LVLEGMC*. https://videscentrs.lvgmc.lv/lapas/sllc-latvian-environment-geology-and-meteorology-centre
7. Wiltink, J. I., Deneke, H., Saint-Drenan, Y.-M., van Heerwaarden, C. C., & Meirink, J. F. (2024). Validating high-resolution global horizontal irradiance retrievals. *Atmospheric Measurement Techniques, 17*, 6003–6026. https://doi.org/10.5194/amt-17-6003-2024
8. Urraca, R., Huld, T., Gracia-Amillo, A., Martínez-de-Pisón, F. J., Kaspar, F., & Sanz-García, A. (2018). Evaluation of GHI estimates from ERA5 and COSMO-REA6 using ground- and satellite-based data over Europe. *Solar Energy, 164*, 339–354. https://doi.org/10.1016/j.solener.2018.02.059
9. Redweik, P., Catita, C., & Brito, M. C. (2013). Solar energy potential on roofs and façades in an urban landscape. *Solar Energy, 97*, 332–341. https://doi.org/10.1016/j.solener.2013.08.036
10. Bill, A., Mohajeri, N., & Scartezzini, J.-L. (2016). 3D model for solar energy potential on buildings from urban LiDAR data. *UDMV 2016*, 51–56. https://doi.org/10.2312/udmv.20161420
11. Jakica, N. (2018). State-of-the-art review of solar design tools and methods for urban microclimate studies. *Renewable and Sustainable Energy Reviews, 81*(Part 1), 1296–1328. https://doi.org/10.1016/j.rser.2017.05.080
12. Kazemian, A., & Xiang, C. (2025). Large-scale analysis of photovoltaic, photovoltaic-thermal, and solar thermal systems in high-density urban environments. *Applied Energy, 401*(Part B), 126765. https://doi.org/10.1016/j.apenergy.2025.126765
13. Hyndman, R. J., & Koehler, A. B. (2006). Another look at measures of forecast accuracy. *International Journal of Forecasting, 22*(4), 679–688. https://doi.org/10.1016/j.ijforecast.2006.03.001
14. de Myttenaere, A., Golden, B., Le Grand, B., & Rossi, F. (2016). Mean absolute percentage error for regression models. *Neurocomputing, 192*, 38–48. https://doi.org/10.1016/j.neucom.2015.12.114
15. Joshi, B.; Kay, M.; Copper, J. K.; & Sproul, A. B. (2019). Evaluation of solar irradiance forecasting skills of the Australian Bureau of Meteorology's ACCESS models. *Solar Energy, 188*, 386–402. https://doi.org/10.1016/j.solener.2019.06.007
16. Lohmann, G. M., & Monahan, A. H. (2018). Effects of temporal averaging on short-term irradiance variability under mixed sky conditions. *Atmospheric Measurement Techniques, 11*, 3131–3144. https://doi.org/10.5194/amt-11-3131-2018
17. Gueymard, C. A. (2018). A review of validation methodologies and statistical performance indicators for modelled solar radiation data. *Solar Energy, 169*, 260–277. https://doi.org/10.1016/j.solener.2018.04.067
18. Draper, N. R., & Smith, H. (1998). *Applied Regression Analysis* (3rd ed.). Wiley.
19. Urbich, I., Bendix, J., & Müller, R. (2020). Development of a seamless forecast for solar radiation using ANAKLIM++. *Remote Sensing, 12*(21), 3672. https://doi.org/10.3390/rs12213672